climation times for the series—that is, the delay times before onset of degradation—always fit the following order:

$$GLY = SARC \leqq IDA < NTA \ll NMIDA$$

Of these substances, IDA, SARC, and GLY were readily used by microorganisms in the river water and began to degrade within 2 days. The length of the acclimation period for NTA, 7 to 14 days, was unaffected by the presence of IDA, SARC, and GLY and indicated that enzyme induction was required for degradation of NTA. In water acclimated to NTA (runs 4 and 5), IDA, SARC, and NTA were degraded within 3 days. We therefore conclude that any buildup of IDA and SARC as a result of NTA breakdown is impossible.

In runs 1 to 3, in which mixtures of all five amino acids were used, NTA was completely degraded long before the system had acclimated to NMIDA. On the other hand, NTA alone (run 10) was degraded with no accumulation of NMIDA. Therefore, NMIDA appears not to be an intermediate in the biodegradation of NTA. The question of whether IDA, SARC, and GLY are such intermediates is not settled (*16*).

Unlike our analytical procedure, the microorganisms present in river water were able to differentiate IDA from *N*-nitrosoIDA; the former compound was always rapidly and completely degraded (runs 1, 2, 3, 5, and 6), while the latter was not degraded in our samples of river water (runs 7 to 9). The presence of *N*-nitrosoIDA, however, did not hinder the degradation of NTA (compare runs 4 and 5 with run 7). If nitrosation of IDA had occurred during any of our biodegradation runs, we would have observed an apparent accumulation of IDA. Such an accumulation was never observed (*17*).

When NTA was added to Meramec River water (run 10) or sequentially added to Detroit River water (Table 1) it was always completely degraded. There was no accumulation of NMIDA, IDA, SARC, GLY, or *N,N*-dimethyl-GLY, and there were no new peaks in the chromatograms. So efficient was NTA degradation by microorganisms present in our river water samples that no clues were obtained about its biodegradation pathway.

CRAIG B. WARREN
EDWARD J. MALEC
Monsanto Company,
St. Louis, Missouri 63166

References and Notes

1. H. M. N. H. Irving and M. G. Miles, *J. Chem. Soc. A* **727**, 1268 (1966); ———, L. D. Petit, *Anal. Chim. Acta* **38**, 475 (1967); L. A. Highfill and M. M. Crutchfield, Monsanto Company, unpublished data (1972).
2. M. Rubin, *Toxicology of Nitrilotriacetic Acid* (Bulletin, Hampshire Chemical Division, W. R. Grace Co., 1963).
3. For a review of NTA toxicology, see S. S. Epstein, Staff Report to Committee on Public Works, U.S. Senate, December 1971; *Environment* **12**, 2 (1970).
4. R. D. Swisher, M. M. Crutchfield, D. W. Caldwell, *Environ. Sci. Technol.* **1**, 820 (1967); H. O. Bouveng, G. Davisson, E. M. Steinberg, *Vatten* **24**, 348 (1968); H. O. Bouveng, P. Solyom, J. Werner, *ibid.*, in press; B. F. Pfeil and G. F. Lee, *Environ. Sci. Technol.* **2**, 543 (1968); K. S. Shumate, J. E. Thompson, J. D. Brookhart, C. L. Dean, *J. Water Pollut. Contr. Fed.* **42**, 631 (1970).
5. J. M. Tiedje and B. B. Mason, *Bacteriol. Proc.* **71**, 1 (1971).
6. R. D. Swisher, E. J. Malec, T. A. Taulli, paper presented at the 163rd national meeting, American Chemical Society, Boston, 1972.
7. W. Lijinsky and S. S. Epstein, *Nature* **225**, 21 (1970), and references therein.
8. J. V. Dubsky and M. Spritzmann, *J. Prakt. Chem.* **96**, 106 (1917).
9. H. Druckrey, R. Preussman, R. Blum, S. Ivankovic, J. Afkham, *Naturwissenshaften* **50**, 100 (1963).
10. C. B. Warren and E. J. Malec, *J. Chromatogr.* **64**, 219 (1972).
11. All biodegradation studies described in this report were done at room temperature (23° ± 2°C). Detroit River water (*p*H 8.0) was collected downstream from Detroit at the water intake of the Detroit Edison plant. Meramec River water (*p*H 8.3) was collected at Valley Park, Mo., 16 km southwest of St. Louis.
12. C. W. Gehrke, K. Kuo, R. W. Zumwalt, *J. Chromatogr.* **57**, 209 (1971), and references cited therein.
13. Nitrosamines are cleaved to amines by alcoholic HCl [P. A. S. Smith, *The Chemistry of Open Chain Organic Nitrogen Compounds* (Benjamin, New York, 1966), vol. 2, p. 473].
14. Y. K. Chau and M. E. Fox, *J. Chromatogr. Sci.* **9**, 271 (1971), and references therein; B. K. Afghan and P. D. Goulden, *Environ. Sci. Technol.* **5**, 601 (1971); D. Murray and D. Povoledo, *J. Fish. Res. Bd. Can.* **28**, 1043 (1971).
15. Another advantage of our gas chromatography procedure is that heavy metal ions do not cause a negative interference. We were able to analyze for all five amino acids in distilled water that contained Cu^{2+}, 3.5 mg/liter, and in distilled water and secondary sewage effluent that contained Pb^{2+}, 0.2 mg/liter; Zn^{2+}, 0.6 mg/liter; Ni^{2+}, 0.2 mg/liter; Cd^{2+}, 0.1 mg/liter; and Fe^{2+}, 5.0 mg/liter. The presence of a large amount of dissolved salts (for example, phosphate buffer) causes the formation of a residue insoluble in a solution of HCl in butanol. The result is incomplete esterification of the amino acids. We recommend the following procedure: dissolve the residue in 1.0 ml of undiluted trifluoroacetic acid, strip off the volatile acid with a stream of nitrogen, and then proceed with the esterification step.
16. J. M. Tiedje and C. B. Warren, unpublished data.
17. No *N*-nitrosoIDA was observed when NTA was degraded in systems containing nitrite ions (R. D. Swisher and C. B. Warren, unpublished data).
18. We thank R. D. Swisher for advice and for the Meramec River samples and W. A. Feiler for a sample of highly purified NTA.

20 September 1971; revised 7 February 1972

Mars: The Lineament Systems

Abstract. *Analysis of the Mariner 4, Mariner 6, and Mariner 7 photographs shows that Mars has at least two distinct types of lineament systems. The most prominent is a well-developed global-type system. The second consists of radial and concentric lineaments associated with the Hellas and south polar basins.*

An investigation of the Mariner 6 and Mariner 7 photographs has established the existence of a well-defined set of lineament systems on Mars. Prior to these missions the presence of a martian lineament system on the scale of 100 km was suggested by Katterfel'd (*1*), who based his conclusions on a study of the Martian canals. Using the Mariner 4 imagery, Binder (*2*) showed that, on the scale of 1 to 10 km, the cratered terrain in Mare Sirenum and Amazonis contains a lineament system whose characteristics are similar to those of a plane-wide system as theoretically investigated by Vening Meinesz (*3*) and to those of the lunar lineament system, known as the lunar grid system, empirically defined by Strom (*4*). The more extensive coverage and better definition provided by the Mariner 6 and Mariner 7 imagery has allowed a more complete and definitive study of the martian lineaments than could be made with the Mariner 4 data.

The photographs used in this study include the final Mariner 4 photographs as well as the new Mariner 6 and Mariner 7 photographs. The former were rectified photographically and the coordinates and orientation of each image were obtained from the Mariner 4 final progress report (*5*). The latter are the computer rectified versions of the maximum discriminability imagery provided by Jet Propulsion Laboratory. The coordinates and orientation of each of the 1969 images were obtained from the Pegasis (*6*).

Because of the comparatively low quality of the Mariner 4 imagery only about 160 lineaments could be positively identified on the eight frames studied. These lineaments consist of linear wall segments of polygonalized craters found on most frames, graben-like features on frame 11, and linear albedo boundaries such as those found on frames 13 and 14.

In contrast, the Mariner 6 and Mariner 7 imagery contains a great number of readily discernible linear features, such as polygonal crater walls (found on almost all the frames showing cratered terrain), linear rilles (frames 6N19, 6N21, and 6N23), linear ridges (on almost all the high-resolution frames), linear albedo boundaries (frame 6N13), and possible fault scarps (frames 6N6 and 6N14).

Over 5000 lineament strikes were measured on certain frames of low and high resolution. All these lineaments are of the above types, and with the possible exception of some linear albedo boundaries they are probably structural features. While the albedo boundaries that we counted may not all represent true structural lineaments, we counted only the boundaries that are obviously related to other linear structural features in their vicinity. Although the lineaments in each of the above categories were counted separately, a discussion of the differences in the azimuthal frequency distributions of the various lineament types is beyond the scope of this report. However, the majority (approximately 90 percent) of the lineaments are polygonal crater walls and ridges. Since the lengths of these linear elements vary by only about a factor of 3 for each resolution (approximately 20 to 60 km on the low-resolution frames and approximately 2 to 6 km on the high-resolution frames), no weighting scheme was used in the construction of the azimuthal frequency or "rose" diagrams given in Fig. 1. The azimuth count interval is 10° for all areas. Also, the data were checked for possible systematic errors resulting from the enhancement of certain trends by the digitizing process or from solar illumination effects. We found no significant biases in the data.

The Mariner 6 and Mariner 7 data demonstrate that the lineaments are expressions of real elements of surface structure that have systematic, preferential trends. If this were not the case, there would be virtually no reason for the rose diagrams obtained from the same regions at the two different resolutions to be the same. The low resolution–high resolution pairs of rose diagrams, C-D and H-I, in Fig. 1 were taken from the cratered terrain, and a comparison within each pair shows that the diagrams are strikingly similar. Over a change of an order of magnitude in resolution, the lineaments within each pair have the same trends, and hence they are real. Also, since these two pairs indicate that, over a difference of a factor of 100 in area between the two resolutions, the lineament patterns are very similar, deviations from the general lineament patterns are significant and are due to real variation in the sample area.

Two and possibly three distinctive types of lineament systems are visible on the Mariner pictures, and the following paragraphs discuss each type separately. The first is thought to be a planet-wide system, as originally suggested by the earlier studies (*1, 2*). The rose diagrams C, D, E, F, H, and I in Fig. 1 apply to the cratered terrain and illustrate the following characteristics of the system: (i) the major trends are, theoretically (*3*), shear directions that are present in all areas;

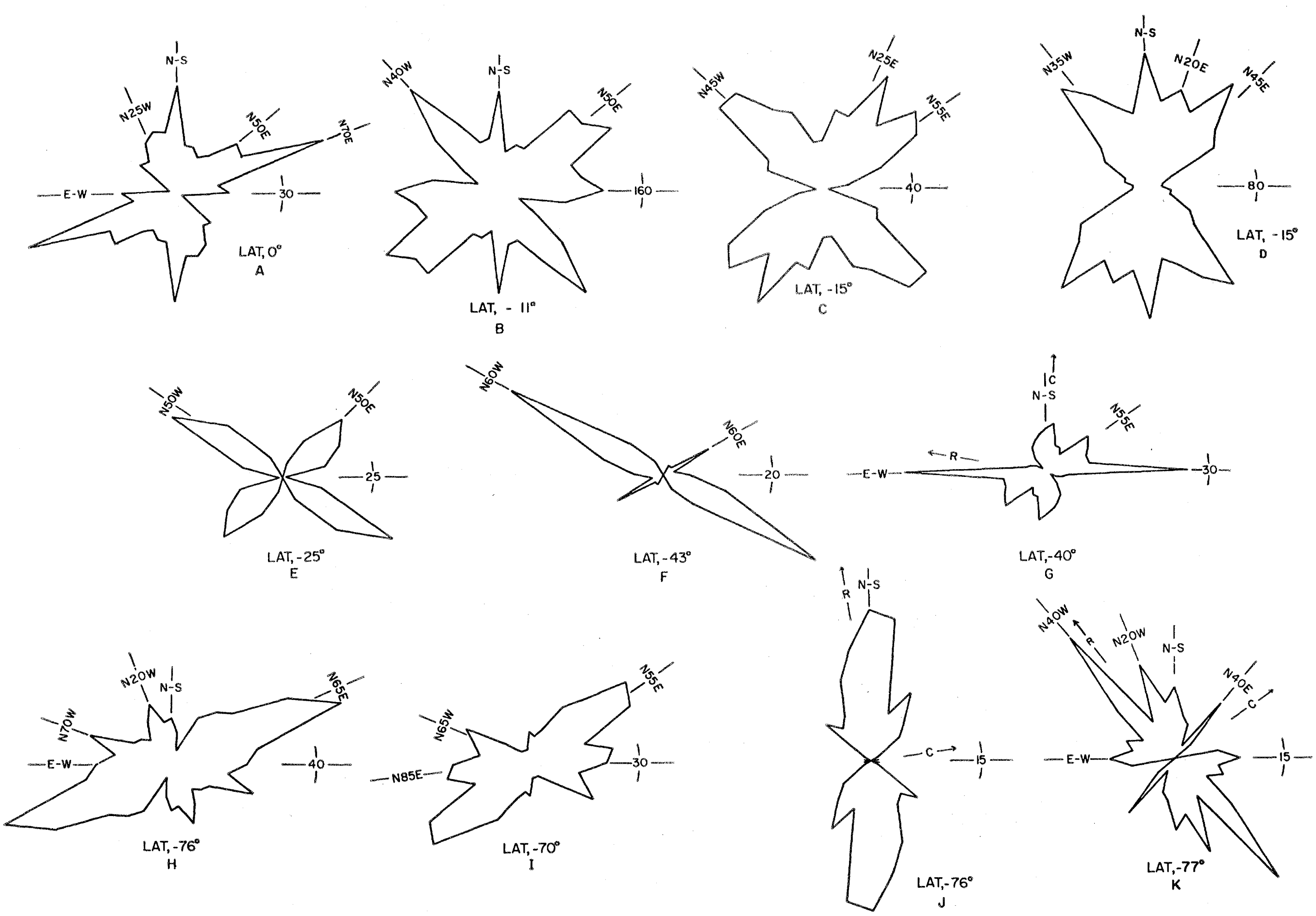

Fig. 1. Rose diagrams depicting the azimuthal frequency of the lineaments for several different areas on Mars. The number enclosed by the E-W marker and the arc at the right of each rose diagram give the radial scale for each diagram, that is, the number of lineaments per 10° count interval at that radial distance from the origin. The strike of each of the significant trends is indicated. In diagrams G, J, and K the radial and concentric directions to the associated basins are designated by lines *R* and *C*.

(ii) the minor trends found in several areas are north to south (N-S), east to west (E-W), 20° to 25° northeast (N20–25E), and 20° to 25° northwest (N25–25W); (iii) the angle between the shears (Δ) increases with latitude. The latter characteristic is illustrated in Fig. 2, which includes values of Δ from the cratered terrain at different latitudes, as well as values of Δ from rose diagram B (which applies to the chaotic terrain and which shows a normal pattern, as discussed below) and from diagram G [here Δ is estimated to be twice the angle between the trend 55° northeast (N55E) and the north direction since the corresponding northwest (NW) trend is not evident]. From Fig. 2, Δ increases from about 90° at 10° latitude to about 130° at 75° latitude; this result is in general accord with the theoretical calculations of Vening Meinesz (*3*). This planet-wide system could be the result of a decrease in the rate of rotation of Mars (*2*), a suggestion that is supported by studies of the angular momenta of the planets (*7*). Alternatively, it could be a result of martian polar wandering (*3*). When more complete photographic coverage of the planet is available from the Mariner 9 orbital mission, it should be possible to distinguish between these two possibilities: if the first suggestion is correct, Δ would vary only with latitude; if polar wandering is the cause of the lineaments, Δ would vary with latitude and longitude (*3*).

The second type of lineament system consists of radial and possibly concentric lineaments associated with the Hellas basin and the basin situated near the South Pole. Diagram G (Fig. 1) represents the lineaments observed in the cratered terrain (low-resolution frame) immediately to the west of Hellas' rim. While the identified trends could all be part of the planet-wide system, two facts strongly suggest that the majority of these lineaments are not part of this system. First, the N-S and E-W trends are more prominent than the shear trend at N55E, and, second, the corresponding N-W shear trend is absent. Since the most prominent trend (E-W) is nearly radial to the center of Hellas and the next most prominent trend (N-S) is nearly concentric to Hellas, we suggest that these lineaments are part of a basin lineament system analogous to the lunar basin systems discussed by Hartmann (*8*). Diagrams J and K apply to the high-resolution frames of areas on and immediately adjacent to the rim of the south polar

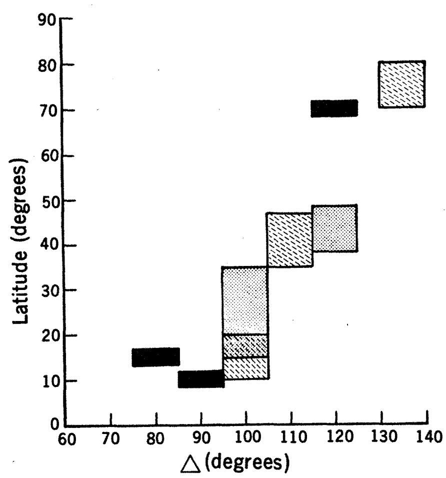

Fig. 2. Variations of Δ, the angle between the shear trends, as a function of latitude. The height of each box indicates the spread in latitude over which the data were taken. The width of each box is an estimate of the uncertainty of the measured Δ. The stippled boxes are the Δ's derived from the Mariner 4 imagery; the hatched boxes are the Δ's derived from the low-resolution Mariner 6 and Mariner 7 imagery; and the filled boxes are the Δ's derived from the high-resolution Mariner 6 and Mariner 7 imagery.

basin, respectively. In both areas the most prominent trend is nearly radial to the center of the basin, and in the case of K a possible concentric trend (N40E) is identified. Thus, these lineaments must also belong to a basin system. This interpretation is supported by the fact that these diagrams in no way resemble diagrams H and I; the former represents the lineament trends of the cratered terrain of the polar area at low resolution, and the latter represents the trends in areas that are far removed from the basin at high resolution.

In diagrams G, J, and K (Fig. 1) the observed radial and concentric trends depart, by about 10° on the average, from the true radial and concentric directions of the basins. This discrepancy might be an artifact of averaging since the azimuth count interval is 10°, it might be due to the present uncertainties in the locations of the pictures and the centers of the basins, or it might result from a combination of both effects. Alternatively, it could be a real effect, since studies of the lunar basin lineament systems have shown that the radial and concentric features tend to be parallel, or nearly parallel, to the lunar grid system where the trends of the grid and the basin systems nearly coincide. Thus, the lunar basin features rarely are truly radial or concentric to the basin, and we might expect the same effect on Mars.

A third possible type of lineament system is illustrated by diagram A (Fig. 1), which represents the lineament trends of the Sinus Meridiani area. This diagram does not fit the planet-wide pattern for this latitude. The Mariner 7 CO_2 topographic data (*9*) show that Sinus Meridiani is a small, low domical feature that lies in a generally low area (*10*). Thus, it seems reasonable to suggest that Sinus Meridiani is the result of local tectonic activity that has also produced a local lineament system younger than and not related to the global system.

Finally, a special study of the high-resolution frames covering the chaotic terrain was made, since this region has probably undergone relatively recent developmental activity (*11*); diagram B (Fig. 1) shows the results. We find that the lineament pattern is similar to that of the nearby cratered terrain (see diagrams C and D). We therefore infer that the chaotic terrain forms by a passive process that utilizes the preexisting crustal fractures of the lineament system. This conclusion is in agreement with the concept that the chaotic terrain is the result of subsidence (*11*).

ALAN B. BINDER
IIT Research Institute,
60 West Giaconda Way,
Tucson, Arizona 85704

DONALD W. MCCARTHY, JR.
IIT Research Institute and
Steward Observatory,
University of Arizona,
Tucson 85721

References and Notes

1. G. N. Katterfel'd, *Izv. Vses. Geogr. Obshch.* **91**, 272 (1959), translated by E. R. Hope (T 445 R, Defense Research Board, Ottawa, Canada, 1966).
2. A. B. Binder, *Science* **152**, 1053 (1966).
3. F. A. Vening Meinesz, *Trans. Amer. Geophys. Union* **28**, 1 (1947).
4. R. G. Strom, *Commun. Lunar Planet. Lab.* **2**, 205 (1964).
5. R. B. Leighton, B. C. Murray, R. P. Sharp, J. D. Allen, R. K. Sloan, *Mariner Mars 1964 Project Report: Television Experiment* (Technical Report 32-884, Jet Propulsion Laboratory, California Institute of Technology, Pasadena, 1967).
6. J. K. Campbell, *Mariner Mars 1969 Simulated TV Pictures (Final)* (JPL 605-237, Jet Propulsion Laboratory, California Institute of Technology, Pasadena, 1970).
7. F. F. Fish, *Icarus* **7**, 251 (1967); W. K. Hartmann and S. M. Larson, *ibid.*, p. 257.
8. W. K. Hartmann, *Commun. Lunar Planet. Lab.* **2**, 1 (1963); *ibid.* **2**, 175 (1964).
9. K. C. Herr, D. Horn, J. M. McAfee, G. C. Pinmental, *Astron. J.* **75**, 883 (1970).
10. A. B. Binder, *Mod. Geol.* **3**, 61 (1972).
11. R. P. Sharp, L. A. Soderblom, B. C. Murray, J. A. Cutts, *J. Geophys. Res.* **76**, 331 (1971).
12. This work was supported by NASA contract NASW-2069.

22 November 1971; revised 7 February 1972